Soft Matter

Accepted Manuscript

ROYAL SOCIETY OF CHEMISTRY

www.rsc.org/softmatter

The dynamics and rheological behavior of colloidal gels under different regimes of oscillatory shear flow have been studied by Brownian dynamics simulation. The dynamics and rheological behavior are discussed in terms of the microstructural change from rigid to soft chain structures.

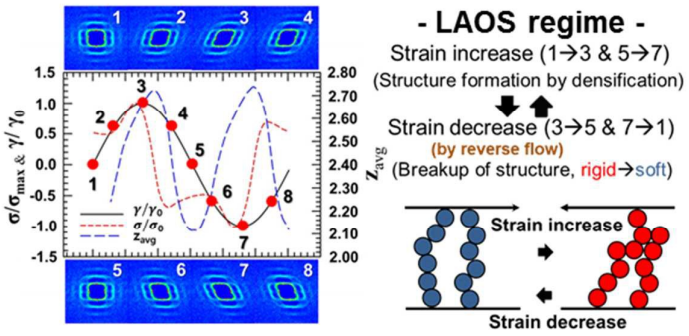

Structural change and dynamics of colloidal gels under oscillatory shear flow

Jun Dong Park, Kyung Hyun Ahn*, Seung Jong Lee

School of Chemical and Biological Engineering, Institute of Chemical Process,

Seoul National University, Seoul, 151-744 Korea

*Corresponding author: ahnnet@snu.ac.kr, Tel.: +82 2 880 8322

Abstract

The dynamics and rheological behavior of colloidal gel under oscillatory shear flow have been studied by using the Brownian dynamics simulations. The dynamics is studied under the oscillatory shear of small, medium, and large amplitude. In the small amplitude oscillatory shear (SAOS) regime, the colloidal gel retains a rigid-chain network structure. The colloidal gel oscillates with small structural fluctuations and the elastic stress shows a linear viscoelastic response. In the medium amplitude oscillatory shear (MAOS) regime, the rigid network structure is ruptured, and a negative correlation between the absolute value of strain and the average bond number is observed. The elastic stress shows a transient behavior in between the SAOS and LAOS responses. In the large amplitude oscillatory shear (LAOS) regime, the colloidal gel shows a soft chain structure. Contrary to the negative correlation in the MAOS regime, the colloidal gel shows an oscillating dynamics with a positive correlation between the absolute value of strain and the average bond number. The soft chain structure exhibits no elasticity at small strain, while it shows strong elasticity at large strain. The oscillating dynamics and the rheological behavior are discussed in terms of the microstructural change from rigid to soft chain structure.

1. Introduction

Attractive colloidal particles arrange themselves to form a variety of microstructures that depend on their concentration and interparticle interactions. At low volume fraction, the particles form fractal aggregates, and they organize to form a fractal colloidal gel as the volume fraction is increased.[1-4] At high volume fraction, the colloidal particles form a closely packed structure, referred to as a colloidal glass.[5-8] The structure and physical properties of the gel and the glass have been studied using the fractal theory and Mode Coupling Theory (MCT). In between the fractal gel at low volume fraction and the colloidal glass at high volume fraction, the particles organize themselves into a colloidal gel with a percolated network structure at intermediate volume fraction ($\geq$ 10%). The complex behavior and physical properties of colloidal gels at intermediate volume fraction have been investigated by various approaches.[1,9-12]

A colloidal gel at intermediate volume fraction, which will be handled in this work, is characterized by a sample-spanning network structure of dynamically-arrested particles.[13-14] The network structure of the colloidal gel imparts solid-like elastic properties which result in complex rheological behavior. In many studies, using theoretical,[15-17] experimental, and simulation approaches, [18-20] the origin of the elasticity has been studied and correlated to the microstructure of the stress-bearing networks. Topological analysis of the colloidal gel demonstrates that the stress-bearing network consists of dynamically arrested particles with high coordination number or bond number. These works suggest a strong correlation between the elasticity and the microstructure. Recently, a numerical study on the aging of colloidal gel gives an insight into the relationship between the elasticity and microstructure.[21] In addition, experimentally, a model gel system has been studied for coordinated measurements of structure and rheology, which is expected to enable more quantitative experimental analysis.[22]

When sufficiently large deformation or stress is applied, the colloidal gel undergoes rupture of microstructure, which is called yielding. The yielding takes forms of various structural changes such as rearrangement, bond rupture, cage breakage, and flow-induced anisotropy.[20,23-26] Depending on the conditions, the colloidal gel shows diverse yielding mechanism. The fractal gels at low volume fraction demonstrates the yielding process of structural reorientation, break-up, and cluster densification under the step shear.[27] In between the two cases of fractal gel at low volume fraction and dense gel at high volume fraction, the colloidal gel at intermediate volume fraction shows a yielding behavior in the sequence of deformation, breakup of the percolated network structure, rotation and breakup of the clusters, and equilibration of the three representative motions of small flocs.[20] At intermediate volume fraction, a new perspective, which regards the yielding of colloidal gel as a

transition from rigid chain to soft chain, has been suggested.[22] In a recent study under the step shear[28], the yielding of the colloidal gel at intermediate volume fraction has been studied in terms of the stress localization and stiffening, which corresponds to stretching and alignment of the network chains. On the other hand, studies under oscillatory shear show two-step yielding behavior. At low concentration, the colloidal gel shows two-step yielding, which is caused by bond rotation and bond breakage.[29] In the case of dense gel at high volume fraction, another two-step yielding behavior of bond breakage and cage breaking has been suggested.[25] Despite all these efforts, the yielding of a colloidal gel is not fully understood yet, especially about its fundamental mechanism.

The yielding behavior, which is caused by the applied deformation or stress, accompanies linear to non-linear transition of the rheological properties.[19-20] This coupling between microstructural change and rheological property changes of colloidal gel has been studied mainly under the dynamic oscillatory shear flow and start-up of shear flow. The latter has been studied using direct visualization,[19] light scattering,[27] and simulation method.[20,30,31] In these studies, the dynamics of colloidal gels were investigated by analyzing the structural evolution under the start-up of shear flow, which directly led to a correlation between the microstructure and rheology. In the case of dynamic oscillatory shear flow, the coupling between the microstructure and rheology was investigated by observing the changes in rheological properties, such as G' and G''. For example, two-step yielding[25,29] was suggested on the basis of G' and G''. However, measuring the rheological properties only is not enough to clearly describe the behavior of colloidal gels. Further, G' and G'' are defined based on a linear response, and they are not sufficient to describe nonlinear stress responses.[32] In addition, the absence of information on the microstructural change makes understanding the response of colloidal gels difficult. Rheo-SANS has also been used to study the microstructure under the dynamic oscillatory shear flow and showed a link between the microstructural change and the rheological behavior.[33,34] However, rheo-SANS gives information only on the averaged microscopic dynamics. The structural change of a colloidal gel under oscillatory shear flow has also been observed by confocal microscopy.[35] However, it was confined to the static structure after oscillatory shear flow rather than the dynamic structural changes during the oscillatory shearing. Considering that the nonlinear response is more closely connected to the dynamic structural changes during the oscillatory shear flow rather than the static structure after the flow, understanding the dynamics of colloidal gels cannot be achieved without grasping the oscillating dynamics. Therefore, there is a need of study on the oscillating dynamics of colloidal gels. In addition, the dependence of nonlinear responses and microstructural changes on various oscillatory shear flows should be studied further, as in the other systems [36,37], and discussed with consideration of the oscillating dynamics.

In this work, we investigate the microstructural changes and the rheological behavior of colloidal gels under dynamic oscillatory shear flow using the Brownian dynamics simulations. Firstly, the microstructures of the colloidal gel under various oscillatory shear conditions (strain amplitude and frequency) are discussed. Depending on the conditions, the colloidal gel presents different microstructures, which manifest themselves with different oscillating dynamics and stress responses. The oscillating dynamics and rheological behavior were explored in three flow regimes of different strain amplitudes; SAOS (small amplitude oscillatory shear), MAOS (medium amplitude oscillatory shear), and LAOS (large amplitude oscillatory shear) regimes. In each regime, the oscillating dynamics was analyzed by investigating the structural fluctuation during the oscillatory shear flow. The structural fluctuations were quantified by the change of average bond number, which effectively describes the topological changes of the colloidal gel. In addition, the structural fluctuations were analyzed in terms of anisotropy using the pair distribution function. The complex stress responses were studied through the stress decomposition method[38] which decomposes the shear stress into elastic and viscous components even in nonlinear regime. By correlating the oscillating dynamics and stress response to the microstructure, the characteristic behavior of colloidal gels at three different flow regimes is discussed.

2. Method

2.1. Simulation

In this work, the Brownian dynamics simulation technique with the concept of surface bonding is introduced to describe the dynamics of colloidal gels. Details about the simulation are fully available elsewhere.[20,30,31,39-41] Therefore, we only discuss the outlines briefly. We consider a three dimensional cubic box where 10,648 monodisperse particles are placed to form a weakly aggregating colloidal gel (20 volume %). The Lee-Edwards boundary condition[42] is applied in all three directions. The governing equations are formulated in terms of the dimensionless parameters. The length is scaled by the radius (a) of the particle, and the energy by the thermal energy (k_BT). The time is scaled with the characteristic time (τ_r) during which the particles diffuse a distance equivalent to the particle radius (a).

$$\tau_r = \frac{a^2}{D^T}. \quad [1]$$

Here, D^T indicates the translational diffusion coefficient of the particle at infinite dilution.

The particle interaction is composed of three potentials; core potential (ϕ_c), bonding potential (ϕ_B), and non-bonded long-range potential (ϕ_N). Firstly, the core potential is used to prevent the overlap of the particles. The core potential, which describes the particle surface, is given by a steep repulsive potential with the potential energy parameter, $K = 4000$.

$$\phi_C(r_{ij}) = \frac{1}{2}K(2a - r_{ij})^2, r_{ij} < 2a$$
$$= 0, r_{ij} \geq 2a \quad [2]$$

Here, r_{ij}, the inter-particle distance is defined as

$$r_{ij} = |\boldsymbol{r_i} - \boldsymbol{r_j}| \quad [3]$$

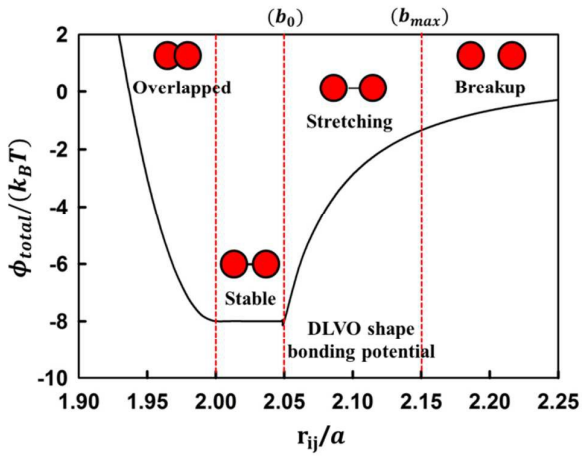

Fig. 1 Pair interaction potential for a collinear extension, in which the bond length between the particle surfaces ($\boldsymbol{b_{ij}}$) corresponds to the surface separation ($\boldsymbol{r_{ij} - 2a}$).[20] The pair interaction potential consists of core potential ($\boldsymbol{\phi_C}$, for $\boldsymbol{r_{ij} < 2a}$), bonding potential ($\boldsymbol{\phi_B}$, for $\boldsymbol{2a \leq r_{ij} \leq 2a + b_{max}}$) and non-bonded long range potential ($\boldsymbol{\phi_N}$, for $\boldsymbol{2a + b_{max} < r_{ij}}$). $\boldsymbol{\phi_B}$ and $\boldsymbol{\phi_N}$ are assumed to have a DLVO shape ($\boldsymbol{a}$=1$\boldsymbol{\mu m}$, $\boldsymbol{A = 3.2 \times 10^{-20} J}$, $\boldsymbol{\varepsilon = 81\varepsilon_0}$ F $\boldsymbol{m^{-1}}$, $\boldsymbol{\psi = 4mV}$, $\boldsymbol{\kappa = 5 \times 10^7\ m^{-1}}$).

As shown in Fig.1, when two particles approach within a critical separation($r_{ij} < 2.15a$), a bond is formed on the particle surface. The bond induces the force and the torque, resulting in translational and rotational motions of the particles. In this work, the bonding potential is a DLVO type given by,

$$\varphi_{DLVO}\left(r_{ij}\right)=\varphi_{vdW}\left(r_{ij}\right)+\varphi_{el}\left(r_{ij}\right) \quad [4]$$

$$\varphi_{vdW}\left(r_{ij}\right)=-\frac{A}{6}\left[\frac{2a^2}{r_{ij}^{\,2}-4a^2}+\frac{2a^2}{r_{ij}^{\,2}}+\ln\left(\frac{r_{ij}^{\,2}-4a^2}{r_{ij}^{\,2}}\right)\right] \quad [5]$$

$$\varphi_{el}\left(r_{ij}\right)=\frac{\varepsilon a\psi^2}{2}\left[\ln\left(1+\exp\left(-\kappa\left(r_{ij}-2a\right)\right)\right)\right]. \quad [6]$$

Here, A, ε, ψ and κ represent the Hamaker constant, the dielectric constant of solvent, the surface potential of the particle, and the Debye screening length, respectively. According to the bond length between the particle surfaces (b_{ij}), the bonding potential is divided into two parts using b_0 (stable region parameter) and (b_{max}) (maximum bond length) as criteria.

$$\begin{aligned}\phi_B\left(b_{ij}\right)&=\varphi_{DLVO}\left(b_0+2a\right) \quad , \quad b_0 \geq b_{ij}\\ &=\varphi_{DLVO}\left(b_{ij}+2a\right) \quad , \quad b_{\max} \geq b_{ij} > b_0\end{aligned} \quad [7]$$

For the bonds with the bond length shorter than b_0, the bonding potential is set to a constant value of $\varphi_{DLVO}(b_0+2a)$ to describe the stable region where no attractive force is assumed. For the bonds with the bond length longer than b_0 and shorter than the maximum bond length (b_{max}), the bonding potential is described as a spring with a DLVO potential.

As the particles are detached from each other, the bond length goes beyond the maximum and they break up. After the break-up, the particle interaction is described by the non-bonded long range interaction $\left(\phi_N(r_{ij})\right)$. This center-to-center inter-particle potential is set as the DLVO potential.

$$\phi_N\left(r_{ij}\right)=\varphi_{DLVO}\left(r_{ij}\right) \quad [8]$$

Bringing these three potentials altogether, the total inter-particle potential is given as a function of the inter-particle distance and the bond length. From the gradient of the total inter-particle potential, we can get the total inter-particle force $(\boldsymbol{F_{ij}})$, by which the translational motion of the particle is described.

$$\begin{aligned}\phi_{total}&=\phi_c\left(r_{ij}\right)+\phi_B\left(b_{ij}\right)+\phi_N\left(r_{ij}\right)\\ \boldsymbol{F_{ij}}&=-\nabla\phi_{total}\left(r_{ij},b_{ij}\right)\end{aligned} \quad [9]$$

In Fig.1, the total pair interaction with this potential is plotted for a case of collinear extension.

The translational motion of the particle is described by the Langevin equation.[42,43]

$$m\frac{d\boldsymbol{v}_i(t)}{dt} = -\xi \boldsymbol{v}_i(t) + \sum_j \boldsymbol{F}_{ij}(t) + \boldsymbol{F}_i^R(t) \quad [10]$$

The first term on the right-hand side describes the hydrodynamic force. In this work, we neglect hydrodynamic interaction, and the Stokes friction coefficient $\xi(=6\pi\eta a)$ is used to describe the drag force by the fluid. The second term represents the inter-particle interaction, and the last term is the random force that describes the thermal motion of the particles. In this work, the inertia term on the left is ignored. We assume the shear flow has a linear profile, meaning that the above Langevin equation is discretized as follows by the Euler method.[43]

$$\boldsymbol{r}_i(t+\Delta t) = \boldsymbol{r}_i(t) + \left[\sum_j \boldsymbol{F}_{ij}(t) + \boldsymbol{F}_i^R(t)\right]\frac{\Delta t}{\xi} + y_i\dot{\gamma}_{xy}\Delta t \quad [11]$$

In this work, $\dot{\gamma}_{xy}$ is given by the time derivative of strain γ, which is sinusoidal as follows

$$\gamma = \gamma_0 \sin(\omega t). \quad [12]$$

The rotational motion of the particle is described by the following equation.[20,39,40]

$$\Delta\boldsymbol{\varphi}_i = \left(\frac{\boldsymbol{T}_i}{\xi_R} + \frac{\boldsymbol{T}_i^R(D^R,t)}{\xi_R}\right)\Delta t \quad [13]$$

Here, $\Delta\boldsymbol{\varphi}_i$ is the total angular displacement and $\boldsymbol{T}_i, \boldsymbol{T}_i^R(D^R,t), \xi_R$ are the inter-particle torque, the random torque by the rotational diffusion, and the rotational friction coefficient, respectively. The torque $\boldsymbol{T}_i(t)$ induced by the inter-particle interaction is given by

$$\boldsymbol{T}_\mathrm{i} = \sum_j \boldsymbol{a}_j \times \boldsymbol{F}_{ij}(t) \quad [14]$$

where $\boldsymbol{a}_j$ represents the position of the *j*-th bond on the surface of *i* particle relative to the *i* particle center. Neglecting multi-body hydrodynamic interaction, the rotational friction coefficient is given by

$$\xi_R = 8\pi\eta a^3. \quad [15]$$

The rotational diffusion of the particle is described by a random torque given by

$$\left|\boldsymbol{T}^R\right| = \left|\frac{\Delta\boldsymbol{\varphi}^R\xi_R}{\Delta t}\right| \quad [16]$$

where $\Delta\boldsymbol{\varphi}^{\boldsymbol{R}}$ is the angular displacement by the rotational diffusion with zero average and the variance of $6D^R\Delta t$ (here, D^R represents the rotational diffusion coefficient).

In this work, all the analysis was conducted and averaged from the results of five different simulations with different initial particle configurations and random motion. In addition, to ensure the steady state condition, the results from the first twenty oscillating cycles were discarded.

2.2 Initial gel structure.

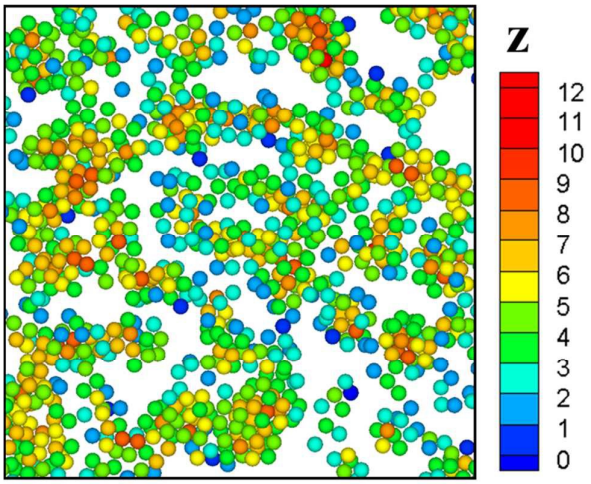

Fig. 2 Initial gel structure at quiescent state. The gel age is $30\boldsymbol{\tau_r}$**.** Particles at the center of the simulation box (sliced with a thickness of 6a in the flow-shear gradient (x-y) plane) are depicted. The color represents the bond number (z) of the particles.

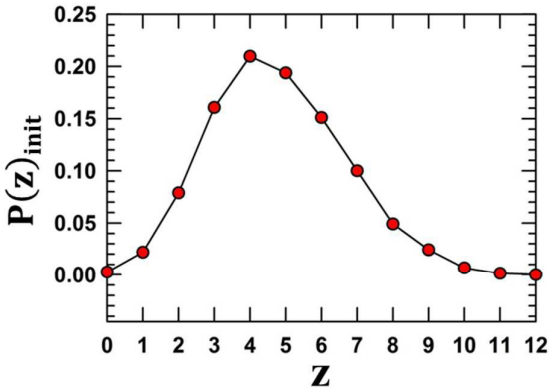

Fig. 3 Initial bond number distribution $\mathbf{P}(\boldsymbol{z})_{\boldsymbol{init}}$.

Initially, the particles were randomly distributed in the simulation box. In the equilibration process without flow, the particles organize themselves into a percolated network structure by thermal fluctuation. After the equilibration process for $30\tau_r$ (3,000,000 steps with 10^{-5} time step), about 99% of the particles out of 10,648 particles were aggregated to form a big single cluster (Fig. S1 in the ESI). The quiescent gel structure is shown in Fig.2, in which the color indicates the number of the particles bonded to each particle, referred to as the bond number, z. In Fig.2, most of the particles are green or yellow, which indicates that the network structure of the colloidal gel mainly consists of rigid chains of particles with bond number larger than or equal to 4. As far as we are concerned, the gel does not show a remarkable aging behavior and the aging does not affect the results significantly. It can be attributed to the surface bonding model used in this work, which prevents the angular reorganization of the particles. The initial structure matches well with that of the experimental work,[19] where the particle system is similar to our simulation condition. In the experimental study using the confocal microscopy, the colloidal gel shows a bond number distribution with a peak around bond number 4 and 5. In addition, about 75% of the particles were experimentally found to have the bond number larger than or equal to 4. In this study, as shown in Fig.3, the peak in the initial bond number distribution ($P(z)_{init}$) is observed around the bond number 4 and 5 in good agreement with the experiments. Moreover, about 75% of the simulated particles have the bond number larger than or equal to 4, which coincides well with the experiments. This means that our simulation describes the quiescent state of a real gel structure effectively. Using both theoretical[15,20] and experimental approaches,[19] previous works revealed that the rigidity of the cluster originates from the microstructure of the particles with bond number larger than or equal to 4 for the particles interacting with non-central or tangential forces as in this simulation. As this rigid structure can be a key determinant of the elasticity of the colloidal gel, the simulations with the realistic quiescent structure are expected to give an effective description of the rheological behavior. In practice, the colloidal gel shows a stress overshoot behavior under the startup of shear, which is one of the important characteristics of the colloidal gel (Fig. S2 in the ESI). In addition, the colloidal gel shows a power-law increase of stress maximum with Pe, which has been observed in previous studies.[22,44]

3. Results and discussion

3.1. Structural change of colloidal gel under oscillatory shear flow

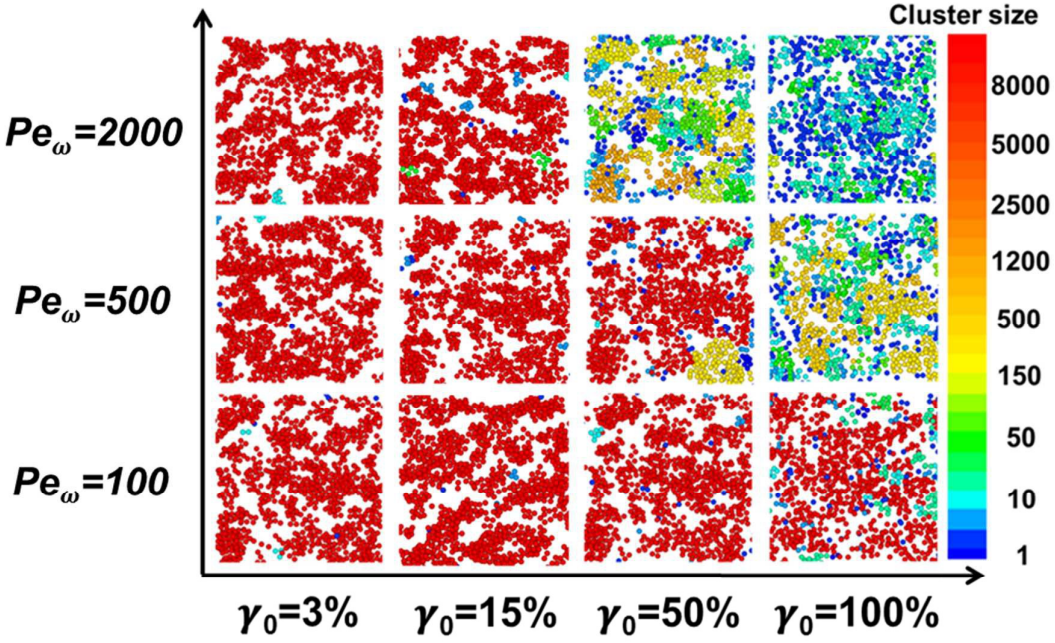

Fig. 4 Structure of a deformed colloidal gel under oscillatory shear flow at maximum strain. The images show the particles at the center of the simulation box (sliced with a thickness of 6a in the flow-shear gradient (x-y) plane). The color indicates the size of the cluster to which the particles belong.

Fig.4 shows the microstructures of the colloidal gels at maximum strain. The abscissa and the ordinate indicate the strain amplitude and frequency, respectively. In this work, the frequency is presented as a non-dimensionalized Peclet number ($\mathrm{Pe}_\omega = \omega\tau_r$), which is the product of the angular frequency (ω) and the characteristic time (τ_r) defined in the previous section.[45] Depending on the flow condition, the colloidal gel shows different structural changes. Regardless of the frequency, at small strain amplitudes, most particles are red, which implies that the colloidal gel maintains its network structure without remarkable structural change. However, at large strain amplitude, 50% and 100%, depending on the frequency, different structural change is observed. At low frequency $\mathrm{Pe}_\omega = 100$, even when the strain amplitude is increased to 100%, the overall network structure is maintained. Nevertheless, the network strands become thinner, which is represented quantitatively by the average bond number decrease in Fig. 5. At frequency of $\mathrm{Pe}_\omega = 500$, as the strain amplitude increases beyond 50%, the colloidal gel starts to break-up into several clusters. Similarly, at high frequency of $\mathrm{Pe}_\omega = 2000$, the increase in strain amplitude results in the rupture of the network structure into small clusters. However, at this high frequency regime, the clusters further breakup into smaller flocs which are colored green and blue in Fig.4. These structural changes can be attributed to different flow conditions which are closely related to the relaxation of flow-induced structural deformation and bond

reformation.[20,25,39] At low frequency, although the imposed large strain deforms the colloidal gel leading to thinner chains, the bond reformation makes it possible to maintain the network structure. However, at high frequency, the colloidal gel is not given enough time for bond reformation.

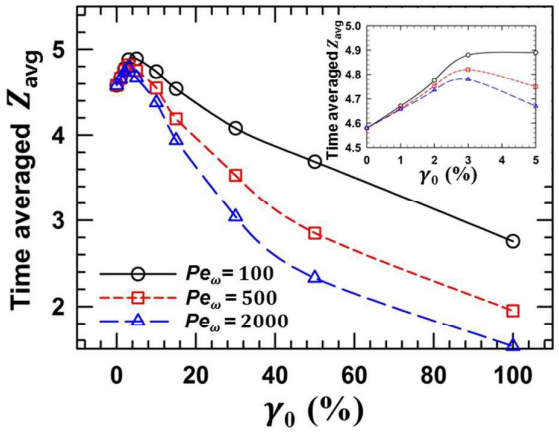

Fig. 5 Time-averaged (during one oscillating cycle) bond number (z_{avg}) as a function of strain amplitude (γ_0). Inset shows the time-averaged bond number change at small strain amplitude regime.

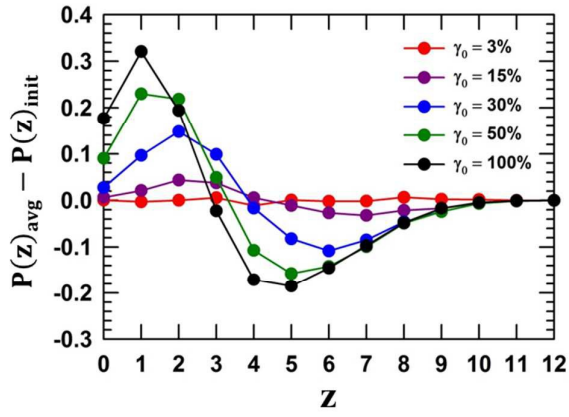

Fig. 6 Time-averaged (during one oscillating cycle) bond number distribution ($\mathbf{P}(z)_{avg}$) change relative to the initial bond number distribution ($\mathbf{P}(z)_{init}$) at frequency $\mathbf{Pe_\omega = 2000}$.

To understand the structural change in local length scale, we calculated the average bond number (z_{avg}) and the bond number distribution change relative to the initial bond number distribution ($P(z)_{avg} - P(z)_{init}$). The average bond number was calculated by dividing the sum of the bond number of the particles by the number of particles. Fig.5 shows z_{avg}, averaged over one

oscillating cycle, as a function of strain amplitude. At small strain amplitude around 3~5%, a slight increase of z_{avg} is observed. It can be considered as a result of shear induced restructuring of the colloidal gel which promotes the aggregation of the particles at low shear rate.[46,47] As the strain amplitude increases further, the z_{avg} starts to decrease, which indicates that the yielding can be regarded as a transition from multiply-connected rigid chains to singly-connected soft chains.[20] In Fig.6, the change in bond number distribution ($\mathrm{P}(z)_{avg} - \mathrm{P}(z)_{init}$) relative to the initial bond number distribution (Fig.3) is shown. As the strain amplitude increases, the fraction of the particles with bond number larger than or equal to 4 decreases, while that of the particles with bond number lower than 4 increases. This structural change corresponds well with that of the previous studies on the start-up of shear flow in which the yielding behavior of the colloidal gel was regarded as a topological change from rigid to soft chains.[19,20] In these studies, the yielding behavior of the colloidal gel was analyzed in terms of the characteristics of the rigid and soft chains. In previous studies[17,19,48], the origin of the elasticity has been attributed to the rigid chain structure. Here, the rigid chain indicates the network structure with high bond number. The particles with high bond number experiences a slow relaxation. Therefore, the particles with high bond number resists against the external deformation supporting the stress. On the other hand, the particles with low bond number experiences fast relaxation and cannot support the stress. Theoretically and experimentally, it has been shown that the criterion for rigidity is the bond number 4, when there is non-central force between the particles as in this work.[15,19] The structural change in this work, the decrease in the particles with bond number larger than or equal to 4 and the increase in the particles with bond number lower than 4, can be understood in the same vein with the previous work. In addition, the observed structural change can be associated with other modeling work. Sticky particle model[49] was employed to study the structural change of attractive particle suspension under the steady shear flow. Under the shear flow, the clusters were disaggregated forming string-like soft chains. The structural changes with sticky particle model can be understood in the context of a transition from rigid chain to soft chain as in this work.

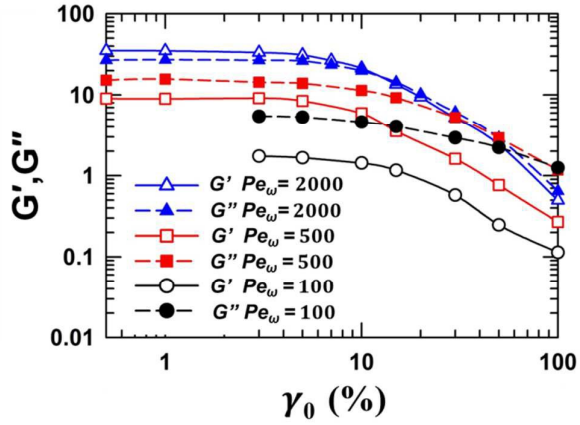

Fig. 7 G′ and G″ as a function of strain amplitude (γ_0).

The structural change from rigid to soft chains is directly manifested in the rheological behavior. Fig.7 shows the storage modulus (G′) and loss modulus (G″) as a function of strain amplitude. They were calculated in the strain amplitude range in which the colloidal gel shows a clear and reasonable stress response. (for example, at $Pe_\omega = 100$, it is hard to get a clear stress curve at strain amplitude lower than 3%) In the small amplitude oscillatory shear (SAOS) (strain amplitude from 0 to 10%), where the rigid chain network is maintained, both G' and G" are almost constant. However, at the medium amplitude oscillatory shear (MAOS) (strain amplitude ~15%), where the structural change from rigid chain structure (with bond number larger or equal to 4) to soft chain structure (with bond number lower than 4) begins to occur, both G′ and G″ start to decrease. In the large amplitude oscillatory shear (LAOS), G′ and G″ decrease as the fraction of the rigid chains decreases.

3.2. Dynamics of colloidal gel under oscillatory shear flow

In this section, the dynamics of the colloidal gel under the oscillatory shear flow at $Pe_\omega = 2{,}000$ will be analyzed. The dynamics will be studied by investigating the structural fluctuation of the colloidal gel which will be quantified by the change of average bond number.

1) SAOS regime

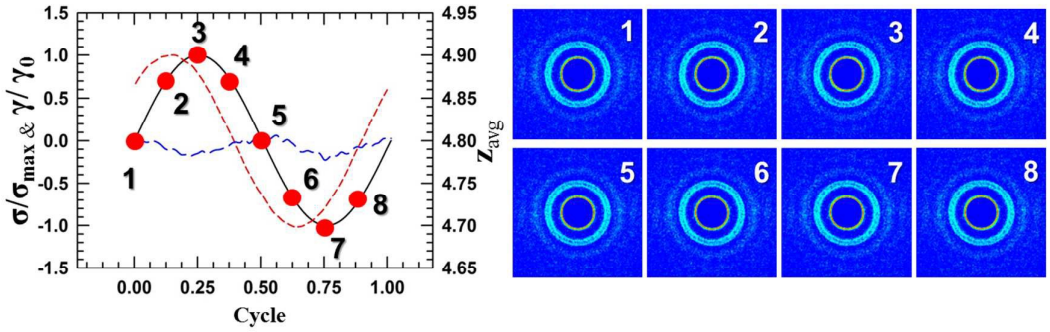

Fig. 8 Normalized stress (σ/σ_{max}, short dashed red line), strain ($\boldsymbol{\gamma/\gamma_0}$, black solid line), and average bond number ($\boldsymbol{z_{avg}}$, long dashed blue line) during one oscillation in SAOS regime ($\boldsymbol{\gamma_0 = 3}$%). Pair distribution functions at every 1/8 cycles (projected onto the flow-shear gradient (x-y) plane) are displayed at the position numbered on the strain curve.

First, we focus on the dynamics of the colloidal gel in the SAOS regime. Fig.8 shows the stress, strain and average bond number in the SAOS regime at a strain amplitude of 3%. The red short-dashed line, black solid line, and blue long-dashed line represent the normalized stress, strain, and average bond number, respectively, in one cycle. At a strain amplitude of 3%, the colloidal gel and displays linear behavior with a sinusoidal stress curve. During the oscillation, the average bond number shows a slight fluctuation and is negatively correlated with the absolute value of strain. As the strain deviates from strain 0 (from point 1 to 3 and from point 5 to 7), the average bond number decreases, while the average bond number increases as the absolute value of strain decreases (from point 3 to 5 and from point 7 to 1). The fluctuation of the average bond number becomes more distinguishable at strain amplitude 5% (Fig. S4 in the ESI). On the right side of Fig.8, the pair distribution functions projected onto the flow-gradient plane at every 1/8 oscillation cycle are given. The pair distribution projection was calculated for a slice of thickness a (particle radius) with the bin size of $\delta r = 0.01a$. In this regime, the colloidal gel shows no anisotropy during the oscillation. In the SAOS regime, it has been shown that the colloidal gel maintains the structure without remarkable structural change. The observed linear behavior with sinusoidal curve can be regarded as a consequence of the maintained rigid network structure.

2) MAOS regime

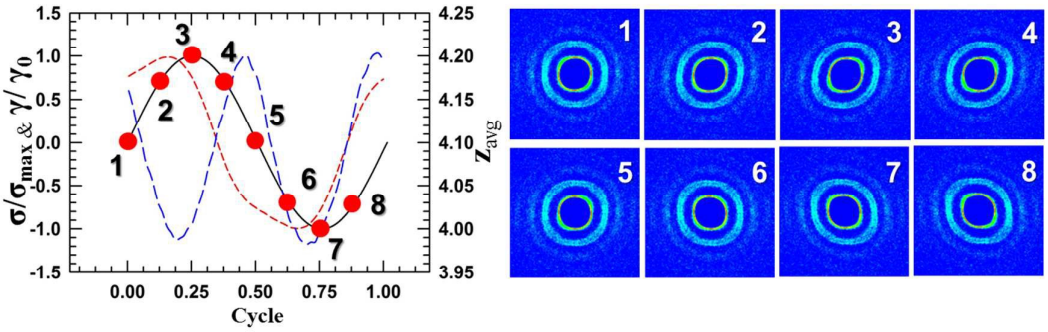

Fig. 9 Normalized stress (σ/σ_{max}, short dashed red line), strain ($\boldsymbol{\gamma/\gamma_0}$, black solid line), and average bond number ($\boldsymbol{z_{avg}}$, long dashed blue line) during one oscillation in MAOS regime ($\boldsymbol{\gamma_0 = 15\%}$). Pair distribution functions at every 1/8 cycles (projected onto the flow-shear gradient (x-y) plane) are displayed at the position numbered on the strain curve.

Secondly, the dynamics in the MAOS regime at strain amplitude of 15% will be discussed. In Fig.9, the stress, strain, and average bond number change under oscillatory shear at a strain amplitude of 15% are shown. Different from the SAOS regime, the colloidal gel shows a clear structural oscillation of the average bond number. As the strain deviates from strain 0 (from point 1 to 3 and from point 5 to 7), the average bond number decreases, while the average bond number increases as the absolute value of strain decreases with the reverse flow (from point 3 to 5 and from point 7 to 1). The dynamics with the negative correlation between the absolute value of strain and the average bond number can be associated with the gel structure as described below. According to the structural change in previous section, a small number of rigid chain starts to break-up into singly-connected soft chains. Both rigid and soft chains coexist in this regime. However, the overall gel structure is still dominated by rigid chains. As the rigid chains resist deformation, the increase in strain will break them into a soft chain structure with less resistance. Therefore, as the absolute value of strain increases, the average bond number decreases. In the reverse flow, as the absolute value of strain decreases, the chain structure is recovered with the increase in the average bond number. This is well manifested in the rheological behavior. In Fig.9, the colloidal gel shows nonlinear behavior with non-sinusoidal stress curve. The stress curve has a shoulder at the point where the average bond number reaches its maximum. The coincidence of these two points implies that the linear-to-nonlinear transition of the colloidal gel can be directly related to the rupture of the network structure. In this regime, as shown in Fig.9, the colloidal gel shows an anisotropic structure. As the absolute value of strain increases, the anisotropy along the compressional axis is observed, which attributes to the structure break-up along the extensional direction. This result is quite similar with that in steady shear

flow.[20,24,33,50] As the absolute value of strain decreases by the reverse flow, the anisotropy decreases and the direction of anisotropy changes according to the strain change.

In the MAOS regime, as the strain amplitude increases, the colloidal gel shows a transition from SAOS to LAOS behavior. (More data at various strain amplitudes in Fig. S4 in the ESI) Near the SAOS regime at strain amplitude 10%, the colloidal gel shows a negative correlation between the absolute value of strain and the average bond number, as in the strain amplitude 15% (Fig. 9). However, as the strain amplitude increases further to 20%, the average bond number changes and the negative correlation disappears. Near the LAOS regime at strain amplitude 30%, the colloidal gel begins to show a positive correlation.

3) LAOS regime

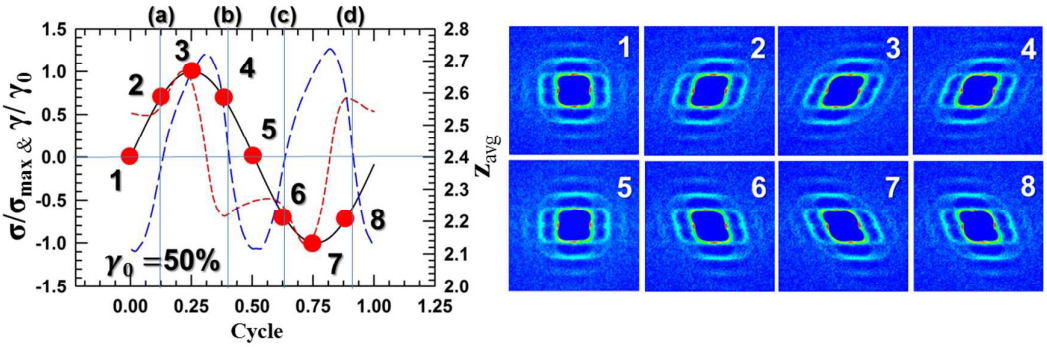

Fig. 10 Normalized stress (σ/σ_{max}, short dashed red line), strain ($\boldsymbol{\gamma/\gamma_0}$, black solid line), and average bond number ($\boldsymbol{z_{avg}}$, long dashed blue line) during one oscillation in LAOS regime ($\boldsymbol{\gamma_0 = 50\%}$). Pair distribution functions at every 1/8 cycles (projected onto the flow-shear gradient (x-y) plane) are displayed at the position numbered on the strain curve.

Lastly, the dynamics in the LAOS regime at strain amplitude of 50% will be considered. In Fig.10, the stress, strain, and average bond number of the colloidal gel under the oscillatory shear flow at strain amplitude 50% are presented. In this condition, the rigid network structure with high bond number is ruptured and the gel structure is dominated by the soft chains with low bond number. The structure shows different dynamics compared to the structure in the SAOS and MAOS regimes. In Fig.10, as the strain deviates from strain 0 (from point 1 to 3 and from point 5 to 7), the average bond number increases, while the average bond number decreases as the absolute value of strain

decreases with the reverse flow (from point 3 to 5 and from point 7 to 1). Compared to the MAOS where the average bond number is negatively correlated with the absolute value of strain, the positive correlation between the average bond number and the absolute value of strain is completely opposite to the previous case. In previous conditions where the gel structure is dominated by the rigid chains, the negative correlation between the absolute value of strain and the average bond number can be associated with the rupture of rigid chain structure which resists deformation. On the other hand, the positive correlation can be associated with the dynamics of soft chains which dominate the overall gel structure in the LAOS regime. Different from the rigid chain, the soft chain shows a floppy motion without resistance against deformation. In the previous study on the dilute colloidal gel with soft chain structure,[29] the floppy motion of the soft chain led to the rotational motion and the bond formation between the soft chains. Therefore, the increase in the average bond number with the absolute value of strain can be ascribed to the shear induced cluster densification by the floppy motion of soft chains. In the reverse flow, the relatively rigid structure which is formed during the increase in the absolute value of strain becomes ruptured, leading to the decrease in the average bond number.

In Fig. 10, the strain and the average bond number are not completely in phase. The average bond number shows a certain phase shift from the strain curve. This shift is observed in the MAOS regime as well. In Fig.9, where the negative correlation is observed, they are not exactly in anti-phase. The phase shift can be attributed to the influence of some remaining rigid or soft chains. In the LAOS regime, the overall structure is dominated by the soft chains which are expected to lead in-phase of both the strain and the average bond number. However, there still exists some rigid chain structure, which is expected to show anti-phase behavior. Therefore, the influence of the remaining rigid structure can be manifested as a phase shift. In the same vein, the phase shift in the MAOS regime, in which the overall structure is dominated by the rigid chains, can be understood as an influence of the soft chains.

In Fig.10, the colloidal gel shows a highly nonlinear stress response with several local maxima and minima. This stress curve is quite similar with that of the experiments where the microstructure and rheology of adhesive hard sphere colloidal gel under large amplitude oscillatory shear has been studied.[33] This highly nonlinear behavior can be related to the structural fluctuation under the oscillatory shear flow. In Fig.10, the average bond number fluctuates between 2.1 and 2.7 with an average value of 2.4. In previous works, [51,52] an average bond number of 2.4 was suggested as a criterion for the rigidity percolation. Considering that this rigidity percolation is closely related to the elastic transition,[52] the average bond number change around 2.4 is expected to have an effect on the rheological response of the colloidal gel. The stress curve in Fig.10 confirms this expectation; at points (b) and (d), as the average bond number decreases below the rigidity percolation (~ 2.4), the colloidal gel loses the elasticity. This is represented by the local minimum (b) and the local maximum

(d) of the stress, which shows a sudden decrease of the stress. On the other hand, at points (a) and (c), as the average bond number begins to rise above the rigidity percolation, the colloidal gel recovers its elasticity. This is expressed as a sudden increase of stress between the point (a) and 3 ((c) and 7).

The pair distribution functions in Fig.10 show the change of structural anisotropy in the LAOS regime. The colloidal gel shows structural anisotropy quite similar with that observed in the MAOS regime. The increase in the absolute value of strain (from point 1 to 3 and from 5 to 7) induces structural anisotropy along the compressional axis, and the decrease in the absolute value of strain (from point 3 to 5 and from 7 to 1) by the reverse flow reduces structural anisotropy. However, compared to that of the MAOS, the colloidal gel shows more anisotropic structure in LAOS. In addition, due to the high shear rate flow, the string structure appears as has been observed previously in the works with hard spheres.[53-55] The formation of a string structure may be attributed to the neglect of hydrodynamic interaction. It means that the hydrodynamic interaction, which is ignored in this study, can be important even for the inter-particle force dominant system. In this sense, the role of hydrodynamic interaction needs to be studied further.

3.3. Stress analysis by stress decomposition

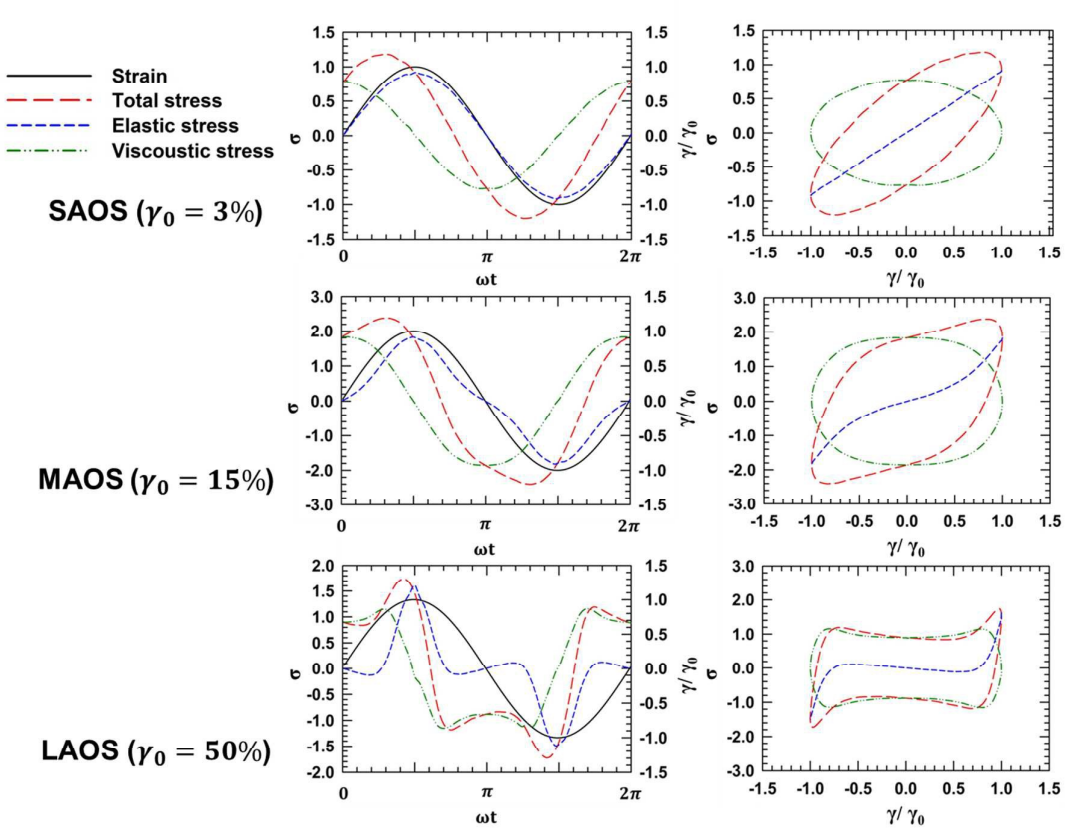

Fig. 11 Stress decomposition and Lissajous curves at three different regimes (SAOS, MAOS, LAOS).

From the Fourier transformation[56-58] to a recent work where the nonlinear behavior is considered as a sequence of physical processes,[59,60] diverse analysis methods have been proposed to interpret the nonlinear response of complex fluids. Among them, in the method with geometrical interpretation of the nonlinear behavior,[38] the response of the material is studied by decomposing the stress signals to elastic and viscous components. In this study, we analyzed the nonlinear stress responses with the stress decomposition method, and associated it with the microstructural change of the colloidal gel.

Fig.11 shows the stress decomposition and the Lissajous curves in each regime. In the first row, the results from the SAOS regime are presented. In the SAOS regime at a strain amplitude of 3%, the elastic stress shows a sinusoidal curve which is in phase with the strain. The viscous stress also shows a sinusoidal curve. This linear behavior is observed in the Lissajous plot as well. The elastic stress is represented by a straight line with a constant slope which reveals the characteristic feature of the linear behavior. In the MAOS regime at a strain amplitude of 15%, a linear- to-nonlinear transition is observed. In the second row of Fig.11, the stress decomposition and the Lissajous curve in the MAOS regime are shown. In this regime, even though the viscous stress demonstrates a sinusoidal

curve as in the SAOS regime, the elastic stress displays a deviation from the sinusoidal curve. Moreover, the elastic stress is not a straight line any more in the Lissajous curve. In the third row in Fig.11, the stress decomposition and the Lissajous curve in the LAOS regime are shown. As in the MAOS regime, the elastic stress does not show the straight line, and the viscous stress is no longer elliptic, which indicates that the nonlinear behavior in the LAOS regime is attributed to both elastic and viscous stresses.

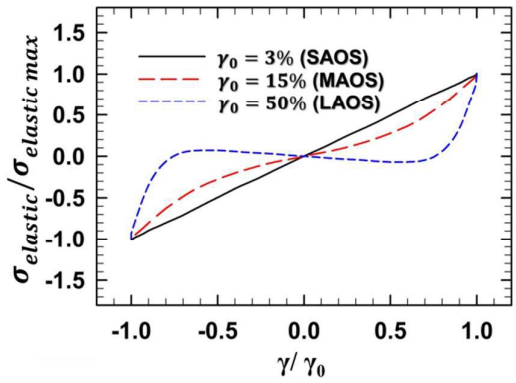

Fig. 12 Normalized elastic stress ($\boldsymbol{\sigma_{elastic}/\sigma_{elastic\ max}}$) as a function of normalized strain ($\boldsymbol{\gamma/\gamma_0}$).

The observed elastic stress can be closely correlated with the microstructure of the colloidal gel. Fig.12 shows the normalized elastic stress ($\sigma_{elastic}/\sigma_{elastic\ max}$) at various strain amplitudes as a function of normalized strain ($\boldsymbol{\gamma/\gamma_0}$). In the SAOS regime, the elastic stress is a straight line with a constant slope. The perfectly elastic behavior can be related to the rigid chain structure in the SAOS regime, where the network structure of the rigid chains is maintained. Because the rigid chain structure with high bond number is the origin of elasticity, the elastic stress which originates from the network of the rigid chains demonstrates the perfectly elastic behavior.

In the LAOS regime, where the colloidal gel consists of singly-connected soft chains, a different behavior is observed. In Fig.12, the elastic stress is divided into two different parts. At large strain, the elastic stress is sensitive to the strain with a steep slope, which represents a strong elasticity. At small strain, the elastic stress shows a nearly plateau which indicates no elasticity. This result can be attributed to the soft chain structure in LAOS regime. According to the structural analysis, in the LAOS regime, the gel structure is ruptured and the initial rigid chain structure turns into the soft chain structure. Different from the rigid chain with high bond number, the soft chain with low bond number shows a floppy motion without resistance to deformation, and the colloidal gel shows no elasticity in the plateau region. However, as the strain increases further, the soft chain starts to stretch and break up at large strain. Therefore, the stretched soft chain, which is the most stress-bearing configuration,[26,28]

demonstrates strong elasticity.

In the MAOS regime, the elastic behavior in between the SAOS and LAOS regime is observed. The elastic stress with strain amplitude of 15% shows two different behaviors. As in the LAOS regime, the colloidal gel shows relatively strong elasticity at large strain compared to small strain. However, unlike the LAOS regime where the elastic stress shows no elasticity at small strain, the elastic stress shows a weak elasticity with a mild slope at small strain. The slope is less steep than that in the SAOS regime. In previous section, it has been shown that some of the rigid chains are ruptured in the MAOS regime and the colloidal gel consists of both rigid and soft chains. At small strain, the remaining rigid network induces elastic behavior as in the SAOS regime. However, compared to the elasticity in the SAOS regime, it demonstrates the relatively weak elasticity due to the rupture of some rigid chains. At large strain, as in the LAOS regime, the elasticity with a nonlinear increase of the elastic stress is observed. This strong elasticity can be thought to be originated from the stretching and breakup of the chain network structure of the colloidal gel.

So far, the stress responses of the colloidal gel in three regimes of SAOS, MAOS, and LAOS have been discussed with the stress decomposition method. However, it should be noted that there exists an argument whether the application of the stress decomposition to yielding systems is appropriate or not.[59-61] For more clear understanding on the nonlinear response of this complex fluid system, more researches with various stress analysis techniques will be necessary. [59-62]

4. Conclusions

The structural changes, oscillating dynamics, and rheological behavior of a colloidal gel under oscillatory shear flow have been explored by the Brownian dynamics simulations. The structural changes of the colloidal gel were quantified by the average bond number, and the oscillating dynamics was studied by investigating the structural fluctuation of the colloidal gel which was quantified by the change of average bond number. The rheological behavior was analyzed by the stress decomposition method. According to the flow conditions, different microstructural changes of the colloidal gel were observed. As the strain amplitude increased, the rigid chain structure with high bond number changed into soft chain structure with low bond number. The characteristic microstructure at each regime manifested itself in the distinctive oscillating dynamics and rheological behavior.

In the SAOS regime where the network structure with rigid chains was retained, the colloidal gel showed the oscillating dynamics with no remarkable structural fluctuation. Although the average

bond number showed a negative correlation with the absolute value of strain, no significant variation of the average bond number was observed during the oscillation. The maintained network structure with rigid chain represented linear rheological behavior.

In the MAOS regime, the rupture of the colloidal gel was observed. The structural change from rigid to soft chains started in this regime, however, the overall structure was still dominated by rigid chains with high bond number. Under oscillatory shear flow, the average bond number decreased with the increase in the absolute value of strain and the average bond number increased with the decrease in the absolute value of strain. The negative correlation between the absolute value of strain and the average bond number could be attributed to the characteristic dynamics of the rigid chains which resists against deformation. In this regime, a linear-to-nonlinear transition, represented by the non-sinusoidal stress curve, was observed. The colloidal gel showed elastic behavior in between the SAOS and LAOS regime.

In the LAOS regime, the colloidal gel showed the microstructure with soft chains. Most of the rigid chain structure ruptured into the singly-connected soft chains which do not resist deformation. Under the oscillatory shear flow, the average bond number increased with the increase in the absolute value of strain and decreased with the decrease in the absolute value of strain. The oscillating dynamics with a positive correlation between the absolute value of strain and the average bond number, which is significantly different from that in previous two regimes, was correlated with the floppy motion of the soft chains. In this regime, both elastic and viscous stresses reflected highly nonlinear rheological behavior. Because of the soft chain structure without elasticity, the elastic stress exhibited no elasticity at small strain. At large strain, the stretching of the soft chain structure induced strong elasticity.

Acknowledgements

The authors are grateful to Simon Rogers, Sunhyung Kim and Norman J. Wagner for stimulating discussions. This work was supported by the National Research Foundation of Korea (NRF) grant (No. 2013R1A2A2A07067387) funded by the Korea government (MEST).

5. References

1. P. J. Lu, E. Zaccarelli, F. Ciulla, A. B. Schofield, F. Sciortino, D. A. Weitz, *Nature*, 2008, **453**, 499

2. E. Zaccarelli, *J. Phys.: Condens. Matter*, 2007, **19**, 323101
3. P. Meakin, *Phys. Rev. Lett*., 1983, **51**, 1119
4. D. A. Weitz, M. Oliveria, *Phys. Rev. Lett*., 1984, **52**, 1433
5. P. J. Lu, D. A. Weitz, *Annu. Rev. Condens. Matter Phys*., 2013, **4**,217
6. N. Koumakis, M. Laurati, S. U. Egelhaaf, J. F. Brady, G. Petekidis, *Phys. Rev. Lett*., 2012, **108**, 098303
7. L. J. Kaufman, D. A. Weitz, *J. Chem. Phys*., 2006, **125**, 074716
8. D. Potoni, T. Narayanan, J. M. Petit, G. Grubel, D. Beysens, *Phys. Rev. Lett*., 2003, **90**, 188301
9. K. Masschaele, J. Fransaer, J. Vermant, *J. Rheol*., 2009, **53**, 1438
10. M. H. Lee, E. M. Furst, *Phys. Rev .E*, 2008, **77**, 041408
11. C. J. Dibble, M. Kogan, M. J. Solomon, *Phys. Rev .E*, 2006, **74**,041403
12. P. Varadan, M. J. Solomon, *Langmuir*, 2003, **19**, 509
13. C. P. Royall, S. R. Williams, T. Ohtsuka, H. Tanaka, *Nature Mater*., 2008, **7**, 556
14. A. I. Campbell, V. J. Anderson, J. S. van Duijneveldt, P. Bartlett, *Phys. Rev. Lett*., 2005, **94**, 208301
15. M. van Hecke, *J. Phys.: Condens. Matter*, 2010, **22**, 033101
16. M. Wyart, H. Liang, A. Kabla, L. Mahadevan, *Phys. Rev. Lett*., 2008, **101**, 215501
17. A.A. Potanin, R. De Rooij, D. Van den Ende, J. Mellema, *J. Chem. Phys*., 1995, **102**, 5845
18. A. D. Dinsmore, V. Prasad, I. Y. Wong, D. A. Weitz, *Phys. Rev. Lett*., 2006, **96**, 185502
19. L. C. Hsiao, R. S. Newman, S. C. Glotzer, M. J. Solomon, *PNAS*, 2012, **109**, 16029
20. J. D. Park, K. H. Ahn, *Soft Matter*, 2013, **9**, 11650
21. R. N. Zia, B. J. Landrum, W. B. Russel, *J. Rheol*., 2014, **58**, 1121
22. L. C. Hsiao, M. J. Solomon, K. A. Whitaker, E. M. Furst, *J. Rheol*., 2014, **58**, 1485
23. J. Vermant, M. J. Solomon, *J. Phys.: Condens. Matter*, 2005, **17**, R187
24. K. Masschaele, J. Fransaer, J. Vermant, *Soft Matter*, 2011, **7**, 7717
25. N. Koumakis, G. Petekidis, *Soft Matter*, 2011, **7**, 2456

26. B. Rajaram, A. Mohraz, *Soft Matter*, 2010, **6**, 2246

27. A. Mohraz, M. J. Solomon, *J. Rheol*., 2005, **49**, 657

28. J. Colombo, E. Del Gado, *J. Rheol*., 2014, **58**, 1089

29. H. K. Chan, A. Mohraz, *Phys. Rev .E*, 2012, **85**,041403

30. M. Whittle, E.Dickinson, *J. Chem. Soc., Faraday Trans*., 1998, **94**, 2453

31. A. A. Rzepiela, J. H. J. van Opheusden, *J. Rheol*., 2004, **48**, 863

32. K. Hyun, M. Wilhelm, C. O. Klein, K. S. Cho, J. G. Nam, K. H. Ahn, S. J. Lee, R. H. Ewoldt, G. H. McKinley, *Prog. Polym. Sci*., 2011, **36**, 1697

33. J. M. Kim, A. P. R. Eberle, A. K. Gurnon, L. Pocar, N. J. Wagner, *J. Rheol*., 2014, **58**, 1301

34. J. T. Kim, A. D. Merger, M. Wilhelm, M. E. Helgeson, *J. Rheol*., 2014, **58**, 1359

35. P. A. Smith, G. Petekidis, S. U. Egelhaaf, W. C. K. Poon, *Phys. Rev .E*, 2012, **76**,041402

36. K. Hyun, J. G. Nam, M. Wilhellm, K. H. Ahn, S. J. Lee, *Rheol. Acta.*, 2006, **45**, 239

37. J. M. Brader, M. Siebenburger, M. Ballauff, K. Reinheimer, M. Wilhelm, S. J. Frey, F. Weysser, M. Fuchs, *Phys. Rev .E*, 2010, **82**,061401

38. K. S. Cho, K. H. Ahn, S. J. Lee, *J. Rheol*., 2005, **49**, 747

39. M. Whittle, E.Dickinson, *Mol. Phys*., 1997, **90**, 739

40. E. Dickinson, *J. Colloid Interface Sci*., 2000, **225**, 2

41. M. Whittle, E.Dickinson, *J. Chem. Phys*., 1997, **107**, 10191

42. A. Satoh, *Introduction to Molecular-Microsimulation of Colloidal Dispersions*, Elsevier, Amsterdam, 2003

43. M. Allen and D. Tildesley, *Computer Simulation of liquids*, Oxford University Press, Oxford, 1987

44. D. Bonn, J. Paredes, M. Denn, L. Berthier, T. Divoux and S. Manneville, arXiv:1502.05281, 2015

45. N. Koumakis, J. F. Brady, G. Petekidis, *Phys. Rev. Lett*., 2013, **110**, 178301

46. C. Selomulya, R. Amal, G. Bushell, T. D. Waite, *J. Colloid Interface Sci*., 2001, **236**, 66

47. V. Oles, *J. Colloid Interface Sci*., 1991, **154**, 351

48. P. Coussot, *Soft Matter*, 2007, **3**, 528

49. D. Chen and M. Doi, *J. Colloid Interface Sci*., 1999, **212**, 286
50. H. Hoekstra, J. Vermant, J. Mewis, G. G. Fuller, *Langmuir*, 2003, **19**, 9134
51. H. He, M. F. Thorpe, *Phys. Rev. Lett*., 1985, **54**, 2107
52. N. E. Valadez-Perez, Y. Liu, A. P. R. Eberle, N. J. Wagner, R. Castaneda-Priego, *Phys. Rev .E*, 2013, **88**, 060302
53. B. Xu, J. F. Gilchrist, *J. Chem. Phys*., 1997, **140**, 204903
54. J. F. Morris, B. Katyal, *Phys. Fluid*, 2002, **14**, 1920
55. D. R. Foss, J. F. Brady, *J. Fluid Mech*., 2000, **407**,167
56. M. Wilhelm, D. Maring, H. W. Spiess, *Rheol. Acta*., 1998, **35**, 399
57. K. Hyun, W. Kim, *Korea-Aust. Rheol. J*., 2011, **23**, 227
58. M. Wilelm, *Macromol. Mater. Eng*., 2002, **287**, 83
59. S. A. Rogers, B. M. Erwin, D. Vlassopoulos, M. Cloitre, *J. Rheol*., 2011, **55**, 435
60. S. A. Rogers, M. P. Lettinga, *J. Rheol*., 2012, **56**, 1
61. A. S. Poulos, J. Stellbrink, G. Petekidis, *Rheol. Acta.*, 2013, **52**, 785
62. R. H, Ewoldt, A. E. Hosoi, G. H. McKinley, *J. Rheol*., 2008, **52**, 1427

List of figures

Fig. 1 Pair interaction potential for a collinear extension, in which the bond length between the particle surfaces ($\boldsymbol{b_{ij}}$) corresponds to the surface separation ($\boldsymbol{r_{ij} - 2a}$). The pair interaction potential consists of core potential ($\boldsymbol{\phi_C}$, for $\boldsymbol{r_{ij} < 2a}$), bonding potential ($\boldsymbol{\phi_B}$, for $\boldsymbol{2a \leq r_{ij} \leq 2a + b_{max}}$) and non-bonded long range potential ($\boldsymbol{\phi_N}$, for $\boldsymbol{2a + b_{max} < r_{ij}}$). $\boldsymbol{\phi_B}$ and $\boldsymbol{\phi_N}$ are assumed to have a DLVO shape ($\boldsymbol{a}$=1$\boldsymbol{\mu m}$, $\boldsymbol{A = 3.2 \times 10^{-20} J}$, $\boldsymbol{\varepsilon = 81\varepsilon_0}$ F $\boldsymbol{m^{-1}}$, $\boldsymbol{\psi = 4mV}$, $\boldsymbol{\kappa = 5 \times 10^7\ m^{-1}}$). Schematic illustrations of bond formation, translational motion and rotational motion of the particles are given in the inset.

Fig. 2 Initial gel structure at quiescent state. Particles at the center of the simulation box (sliced with a thickness of 6a in the flow-shear gradient (x-y) plane) are depicted. The color represents the bond number (z) of the particles.

Fig. 3 Initial bond number distribution $\boldsymbol{P(z)_{init}}$.

Fig. 4 Structure of a deformed colloidal gel under oscillatory shear flow. The images show the particles at the center of the simulation box (sliced with a thickness of 6a in the flow-shear gradient (x-y) plane). The color indicates the size of the cluster to which the particles belong.

Fig. 5 Time-averaged (during oscillation cycle) bond number (z_{avg}) as a function of strain amplitude (γ_0).

Fig. 6 Time-averaged (during oscillation cycle) bond number distribution ($\boldsymbol{P(z)_{avg}}$) change relative to the initial bond number distribution ($\boldsymbol{P(z)_{init}}$).

Fig. 7 G′ and G″ as a function of the strain amplitude ($\boldsymbol{\gamma_0}$).

Fig. 8 Normalized stress (σ/σ_{max}, short dashed red line), strain ($\boldsymbol{\gamma/\gamma_0}$, black solid line), and average bond number ($\boldsymbol{z_{avg}}$, long dashed blue line) change in SAOS regime ($\boldsymbol{\gamma_0 = 3\%}$). Pair distribution functions at every 1/8 cycles (projected onto the flow-shear gradient (x-y) plane) are displayed at the position numbered on the strain curve.

Fig. 9 Normalized stress (σ/σ_{max}, short dashed red line), strain ($\boldsymbol{\gamma/\gamma_0}$, black solid line), and average bond number ($\boldsymbol{z_{avg}}$, long dashed blue line) change in MAOS regime ($\boldsymbol{\gamma_0 = 15\%}$). Pair distribution functions at every 1/8 cycles (projected onto the flow-shear gradient (x-y) plane) are displayed at the position numbered on the strain curve.

Fig. 10 Normalized stress (σ/σ_{max}, short dashed red line), strain ($\boldsymbol{\gamma/\gamma_0}$, black solid line), and average bond number ($\boldsymbol{z_{avg}}$, long dashed blue line) change in LAOS regime ($\boldsymbol{\gamma_0 = 50\%}$). Pair distribution functions at every 1/8 cycles (projected onto the flow-shear gradient (x-y) plane) are displayed at the position numbered on the strain curve.

Fig. 11 Stress decomposition results and Lissajous curves at three different regimes (SAOS, MAOS, LAOS).

Fig. 12 Normalized elastic stress ($\boldsymbol{\sigma_{elastic}/\sigma_{elastic\,max}}$) as a function of normalized strain ($\boldsymbol{\gamma/\gamma_0}$).